Journal of Electrical and Computer Engineering Innovations
(JECEI)
Journal homepage: http://www.jecei.sru.ac.ir

Research paper

Fault Diagnosis of a Permanent Magnet Synchronous Generator Wind Turbine

S. Khodakaramzadeh, M. Ayati*, M.R. Ha'iri-Yazdi

Department of Mechanical Engineering, University of Tehran, Tehran, Iran.

Article Info

Article History:
Received 09 June 2020
Reviewed 23 August 2020
Revised 08 October 2020
Accepted 15 December 2020

Keywords:
Wind energy conversion system (WECS)
Fault diagnosis of wind turbine
Permanent magnet synchronous generator (PMSG) wind turbine
Blade imbalance fault (BIF)
Terminal sliding mode observer (TSMO)

*Corresponding Author's Email Address:
m.ayati@ut.ac.ir

Abstract

Background and Objectives: Designing a terminal sliding mode observer (TSMO) in order to estimate the potential faults in a wind turbine with a doubly fed induction generator (DFIG) has been studied in previous research works. In this paper, a method for fault detection of a permanent magnet synchronous generator (PMSG) wind turbine using a TSMO is developed.
Methods: The wind turbine (WT) dynamic model including, blades, drive train, $3kw$ PMSG, maximum power capture controller, and pitch controller is linearized around its equilibrium point and is simulated in MATLAB Simulink. A PID controller is designed for capturing the maximum power from wind. Also, a PI controller is designed in order to control the pitch angle. In this research, the blade imbalance fault (BIF), which is due to the difference between turbine blades' mass distribution, is investigated. This fault may happen over time and causes rotor mass imbalance that leads to vibrations in the generator's shaft rotating speed. A fault detection system (FDS) is proposed using a terminal sliding mode observer in order to diagnose the BIF.
Results: Using the designed TSMO, the estimation errors of not only measured states but also unmeasured states converge to zero in finite time. This leads to the fast action of the FDS before a failure happens. Using the proposed FDS, the states and fault are estimated such that the estimation errors of states and the fault converge to zero in 0.033 seconds.
Conclusion: The convergence of state estimation errors to zero in finite time, which is verified by simulation results, satisfies the authors' expectation that using TSMO, the estimation errors of both output and non-output states converge to zero in finite time.

Introduction

Wind turbine, which is a type of renewable energy systems, is excited by a random wind profile. Among characteristics of this system are nonlinear dynamics, operation in an uncertain environment, and the dependence of the wind turbine power on geographical and weather conditions [1], [2]. Installation errors, manufacturing deficiencies or aging effects, and challenging environmental conditions are common reasons for the shut-down condition [3].

Overall, a wind turbine is in shut-down condition for 0.595% to 2.705% of a year. Wind turbines are mostly located in remote areas. In addition, performing inspection and maintenance work on WTs is problematic due to the height of the turbine. Therefore, WTs requiring less maintenance are desirable. Moreover, because of complications of a WT system and also due to variations of wind speed, the fault occurrence probability of this system is high. Hence, minimization of the adverse economic effects of the faults is a challenging problem [4], [5]. Concerning the probability of failure occurrence in a wind energy conversion system (WECS) such as the fraction of gear, drive train, and bearing, condition monitoring and fault detection have an essential role in reducing maintenance costs [6]. For a turbine with more than 20 years of operation, the operation and maintenance (OM) and components costs are estimated to be around 10-15% of the total wind farm income. Although larger turbines have fewer OM costs per unit of power, failure costs are higher for these turbines. Therefore, condition monitoring and fault diagnosis are profitable [7]. Furthermore, fault detection in primitive levels and repairing faulty parts in a timely manner is essential for maintenance costs, component costs, downtime reduction, and preventing catastrophic damages [8]. Fault detection in fault-tolerant systems is vital because it provides the required information for fault isolation and system reconfiguration [9]. Modern wind turbines that take advantage of fault diagnosis and fault-tolerant schemes are highly reliable. They operate efficiently and produce economic electrical energy [10]. Due to simple mechanical structures, light weight, high power density, high efficiency, and high reliability of PMSGs, these types of generators are often installed on wind turbines [11], [12]. Moreover, other desired features of PMSGs are their fast dynamical response and low noise [13]. Using an observer for state estimation and fault detection is one of the most useful approaches in wind turbine FDS.

Blades are of weakest parts of a wind turbine. Some faults may occur directly on blades such as hub or blade corrosion/crack and rotor imbalance [6]. Blade bending moment sensor fault, blade root bending sensor fault, and pitch actuator fault are examples of faults that occur in blade sensors and actuators [14]. Pitch dynamic that has hydraulic nature may change because of pressure drop, which occurs in the hydraulic supply system or additional air in the oil [15].

The imbalance fault of the generator shaft causes an additional force in the shaft. The blade imbalance fault in which the mass distribution of one blade is different from other blades causes rotor mass imbalance, which leads to vibrations in the generator's shaft rotating speed [16]. Blade imbalance mainly occurs due to the construction or manufacturing errors, icing condition, and degradation as a result of aging [17]. A fault detection method based on adaptive fuzzy Q-learning (FQL) for PMSG WT blade imbalance fault detection, which is proposed in [18], has 99.9% classification accuracy and uses 3999 samples of generator's current signals. The advantage of this method is that it needs no prior knowledge of the system for fault detection however, it is limited to the working condition of the sampled signals. Blade imbalance fault detection using gene expression programming (GEP) based classifier and empirical mode decomposition (EMD) has been studied in [19].

In this study, blade imbalance fault detection within a PMSG wind turbine is studied. For this purpose, a terminal sliding mode observer (TSMO) is designed for the wind turbine system including blades, drive train, and PMSG with nonlinear dynamics, which estimates both output and non-output states in a finite time. Therefore, TSMO estimates all states and BIF in a finite time.

In the next section, the complete dynamic model of the WECS is explained. In third section, the TSMO's equations, the linearized state-space equations of WECS, and the fault estimation method are described. The complete WECS model including wind turbine, PMSG, controller, and fault models is simulated in MATLAB Simulink and the simulation results are represented in the next section. Finally, last section concludes the research.

Wind Turbine Dynamic Model

The WECS includes a wind turbine, a PMSG, and two controllers. In order to detect the WT's faults, it is necessary to obtain the dynamic equations of the entire system including the WT, the PMSG, the controllers, and the fault. In the following subsection, the dynamic model of the entire WECS is explained.

A. System's Dynamic Model

In this section, the WECS dynamic model including dynamic equations of the wind turbine, the PMSG, the controllers, and BIF is explained. The WECS has four states, two inputs, and one output. The state variables vector is $x=[x_1 \quad x_2 \quad x_3 \quad x_4]^T=[i_d \quad i_q \quad \beta \quad \omega_g]^T$. The dynamical equations of i_d, i_q, ω_g, and β are presented based on Boulouma et al. [20] and Tong and Zhao studies [21]. The input control signals vector is: $u=\begin{bmatrix}R_L & \beta_{ref}\end{bmatrix}^T$ and output is $y=\omega_g$.

The state-space equations are given in (1). In this equation, i_d and i_q are the stator current's d/q components. L_d and L_q are inductances of the stator. R_s is the stator resistance. Φ_m is the linkage flux. P is the number of pole pairs. ω_g is the generator speed. The power electronics and load with highly fast dynamic in comparison to other parts are represented by an equivalent load with constant inductance L_L and the adjustable resistance R_L. τ_β is the pitch actuator's time constant. β is the pitch angle. β_{ref} is the pitch reference angle which is also the pitch controller's output and also the second control input of the wind turbine system. η is the gearbox efficiency. ρ is the air density. The radius of the rotor swept area is represented by R. v is the wind speed. $C_T(\lambda,\beta)$ is the torque coefficient. N_g is the gear ratio. The equivalent inertia transformed into the generator side is represented by J_h. λ is the tip speed ratio (TSR).

$$
\begin{bmatrix} \dot{x}_1 \\ \dot{x}_2 \\ \dot{x}_3 \\ \dot{x}_4 \end{bmatrix} = \begin{bmatrix} -\dfrac{R_s}{L_d+L_L}x_1 + \dfrac{P(L_q-L_L)}{L_d+L_L}x_2x_4 \\ -\dfrac{R_s}{L_q+L_L}x_2 - \dfrac{P(L_d+L_L)}{L_q+L_L}x_1x_4 + \dfrac{P\Phi_m}{L_q+L_L}x_4 \\ -\dfrac{1}{\tau_\beta}x_3 \\ \dfrac{\eta\pi\rho R^3 v^2}{2N_gJ_h}C_T(x_3,x_4) - \dfrac{P\Phi_m}{J_h}x_2 \end{bmatrix}
+ \begin{bmatrix} -\dfrac{1}{L_d+L_L}x_1 & 0 \\ -\dfrac{1}{L_q+L_L}x_2 & 0 \\ 0 & \dfrac{1}{\tau_\beta} \\ 0 & 0 \end{bmatrix} \begin{bmatrix} R_L \\ \beta_{ref} \end{bmatrix} \tag{1}
$$

$$
y = \begin{bmatrix} 0 & 0 & 0 & 1 \end{bmatrix} \begin{bmatrix} x_1 \\ x_2 \\ x_3 \\ x_4 \end{bmatrix}
$$

$$
\tau_\beta = \frac{\beta_{ref}-\beta}{\dfrac{d\beta}{dt}}
$$

B. WT Closed-loop System

In this system, two controllers including a maximum power capture controller and a pitch controller are designed separately, as shown in Fig. 1. In the maximum power capture controller design, the first, second, and fourth states have participated. The third state is considered in the pitch controller design.

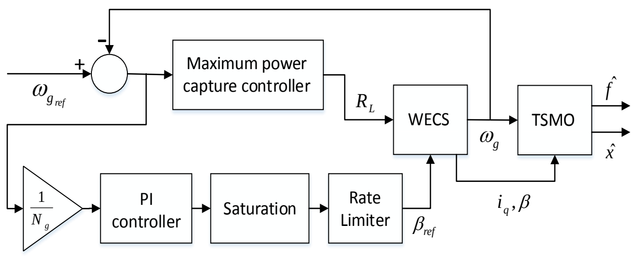

Fig. 1: Block diagram of WECS with maximum power capture controller, pitch controller, and TSMO.

$\omega_{g_{ref}}$ is calculated in order that TSR is maintained close or equal to its optimal value to capture maximum power. β_{ref} and R_L are the control inputs.

B.1: Maximum Power Capture Controller

A PID controller is considered for maximum power capturing as follows:

$$
G_{CMP}(s) = P + I\frac{1}{s} + D\frac{N}{1+N\dfrac{1}{s}} \tag{2}
$$

In the above equation, P is the proportional term, I is considered as the integral coefficient, the derivative coefficient is represented by D, and N is the filter coefficient.

B.2: Pitch Controller

The pitch controller is implemented in the third state equation of (1). The difference between actual power and maximum allowable power is being used to calculate the required pitch angle [22]. In order to control the pitch angle, a PI controller, a rate limiter, and a saturation function are used. The equation of the controller is as follows:

$$
G_{CP}(s) = \frac{\beta_{ref}}{\omega_{r_{ref}} - \omega_r} = k_p + \frac{k_i}{s} \tag{3}
$$

β_{ref} is the pitch reference angle, ω_r is the rotor speed, $\omega_{r_{ref}}$ is the reference rotor speed, k_p and k_i are the PI controller proportional and integral coefficients, respectively.

C. Model Linearization

For the sake of simplicity, the state-space equation's coefficients are defined as:

$$
a_s = -\frac{R_s}{L_d+L_L},\quad b_s = \frac{P(L_q-L_L)}{L_d+L_L},\quad c_s = -\frac{1}{L_d+L_L}
$$

$$
d_s = -\frac{R_s}{L_q+L_L},\quad f_s = -\frac{P(L_d+L_L)}{L_q+L_L},\quad g_s = \frac{P\Phi_m}{L_q+L_L}
$$

$$
h_s = -\frac{1}{L_q+L_L},\ p_s = -\frac{1}{\tau_\beta},\ m_sC_T = \frac{\eta\pi\rho R^3 v^2}{2N_gJ_h}C_T(\lambda,\beta),
$$

$$
n_s = -\frac{P\Phi_m}{J_h}.
$$

Computing Jacobian matrix, the linearized state-space is:

$$
\begin{bmatrix} \dot{x}_1 \\ \dot{x}_2 \\ \dot{x}_3 \\ \dot{x}_4 \end{bmatrix} = \begin{bmatrix} a_s & b_sx_{40} & 0 & b_sx_{20} \\ f_sx_{40} & d_s & 0 & f_sx_{10}+g_s \\ 0 & 0 & p_s & 0 \\ 0 & n_s & m_s\left.\dfrac{\partial C_T}{\partial x_3}\right|_{\substack{x=x_0\\u=u_0}} & m_s\left.\dfrac{\partial C_T}{\partial x_4}\right|_{\substack{x=x_0\\u=u_0}} \end{bmatrix} \begin{bmatrix} x_1 \\ x_2 \\ x_3 \\ x_4 \end{bmatrix}
+ \begin{bmatrix} c_sx_{10} & 0 \\ h_sx_{20} & 0 \\ 0 & -p_s \\ 0 & 0 \end{bmatrix} \begin{bmatrix} u_1 \\ u_2 \end{bmatrix} \tag{4}
$$

where $x_0 = \begin{bmatrix} x_{10} & x_{20} & x_{30} & x_{40} \end{bmatrix}^T$ is the equilibrium point, which is determined by solving the following set of equations:

$$\begin{cases} a_s x_{10} + b_s x_{20} x_{40} = 0 \\ d_s x_{20} + f_s x_{10} x_{40} + g_s x_{40} = 0 \\ p_s x_{30} = 0 \\ m_s C_T(x_{30}, x_{40}) + n_s x_{20} = 0 \end{cases} \tag{5}$$

D. Blade Imbalance Fault Dynamic Model

When blade imbalance fault occurs, the frequency f_r ($1P$ frequency) of the turbine shaft torque variates. Therefore, the turbine shaft torque in the existence of blade imbalance fault equals to:

$$T(t) = T_0 + T_v \cos(2\pi f_r t) \tag{6}$$

T is the turbine shaft torque, T_0 is the torque due to the wind power, and T_v is the amplitude of the shaft torque variations as a consequence of blade imbalance fault [23]. Hence, when blade imbalance fault exists, the state-space equations of (4) are changed as follows:

$$\begin{bmatrix} \dot{x}_1 \\ \dot{x}_2 \\ \dot{x}_3 \\ \dot{x}_4 \end{bmatrix} = \begin{bmatrix} a_s & b_s x_{40} & 0 & b_s x_{20} \\ f_s x_{40} & d_s & 0 & f_s x_{10} + g_s \\ 0 & 0 & p_s & 0 \\ 0 & n_s & m_s \left.\dfrac{\partial C_T}{\partial x_3}\right|_{\substack{x = x_0 \\ u = u_0}} & m_s \left.\dfrac{\partial C_T}{\partial x_4}\right|_{\substack{x = x_0 \\ u = u_0}} \end{bmatrix} \begin{bmatrix} x_1 \\ x_2 \\ x_3 \\ x_4 \end{bmatrix} + \begin{bmatrix} c_s x_{10} & 0 \\ h_s x_{20} & 0 \\ 0 & -p_s \\ 0 & 0 \end{bmatrix} \begin{bmatrix} u_1 \\ u_2 \end{bmatrix} + \begin{bmatrix} 0 \\ 0 \\ 0 \\ 1 \end{bmatrix} f_{BIF} \tag{7}$$

Substituting (6) into state-space equations of (1) and (4), f_{BIF} is obtained as follows:

$$f_{BIF} = \frac{\eta}{N_g J_h} T_v \cos(2\pi f_r t) \tag{8}$$

Terminal Sliding Mode Observer (TSMO) Design

Classical sliding mode observers are widely used for output and state estimations of linear/nonlinear systems in practical researches because of their intrinsic robustness to the uncertainties. The output estimation errors' convergences in a finite time are guaranteed by classical sliding mode observers, while non-output errors converge to zero asymptotically. This means states not directly affected by the output converge to the actual values in infinite time. Hence, terminal sliding mode observers are developed, which guarantee convergence of both output (measured) and non-output (unmeasured) state estimation errors in a finite time [24].

A. TSMO Implementation on WECS

In this section, TSMO is implemented on the linearized system [24], [25]. Primarily, the linearized system model is considered and conditions for state and fault estimation are mentioned. Then, the coordinate is transformed and system and observer equations in the new coordinate system are obtained and design parameters are introduced. Finally, the observer equation is obtained in the original coordinate and fault is estimated.

A.1: Linearized State Model

Consider the time-invariant linear system as follows:

$$\begin{cases} \dot{x}(t) = \bar{A}_L x(t) + \bar{B} u(t) + \bar{F}_a f_a(x,t) \\ \quad y(t) = \bar{C} x(t) \end{cases} \tag{9}$$

In this system n is the number of states, m is the number of control inputs, p is the number of outputs, and q is the number of faults. f_a is the fault vector and $\bar{F}_a$ is the fault intensity matrix. It is supposed that $\|f_a\| \le \gamma$ and the system is observable. The Matrices $\bar{C}$ and $\bar{F}_a$ must be full-rank. Also, the following assumptions must be held.

$$\begin{aligned} &A_1 : rank(\bar{C}\bar{F}_a) = rank(\bar{F}_a) = q \\ &A_2 : 2p \ge n + q \end{aligned} \tag{10}$$

The transformation matrix T_L has the structure:

$$T_L = \begin{bmatrix} T_1 & T_2 & 0 & 0 \\ 0 & 1 & 0 & 0 \\ 0 & 0 & 1 & 0 \\ 0 & 0 & 0 & 1 \end{bmatrix} \tag{11}$$

T_1 and T_2 must be chosen such that the following inequality holds:

$$\bar{a}_{11} + \bar{a}_{21} \frac{T_2}{T_1} < 0 \tag{12}$$

In the above equation, $\bar{a}_{11}$ and $\bar{a}_{21}$ are the first and second elements of the first column of the matrix $\bar{A}_L$. Using the transformation matrix T_L, changing of coordinate is done and the new state matrices are obtained as follows:

$$\begin{aligned} &A_L = \begin{bmatrix} A_1 & A_2 \\ A_3 & A_4 \end{bmatrix}, A_3 = \begin{bmatrix} A_{31} \\ A_{32} \end{bmatrix}, B = \begin{bmatrix} B_1 \\ B_2 \end{bmatrix}, \\ &F_a = \bar{F}_a = \begin{bmatrix} F_1 \\ F_2 \end{bmatrix}, C = \bar{C} = \begin{bmatrix} 0 & C_2 \end{bmatrix} \end{aligned} \tag{13}$$

where:

$A_1 \in R^{(n-p)\times(n-p)}, A_3 \in R^{p\times(n-p)}, A_{31} \in R^{(n-p)\times(n-p)}$,
$F_1 \in R^{(n-p)\times q}, F_2 \in R^{p\times q}, C_2 \in R^{p\times p}$

$F_1 = 0_{(n-p)\times q}, F_2 = \begin{bmatrix} 0_{(p-1)\times q} \\ 1_{1\times q} \end{bmatrix}$.

C_2 is a full-rank matrix. A_{31} is full-rank because the system is observable. Hence, the system state equations are transformed as follows:

$$\begin{cases} \dot{z}_1(t) = A_1 z_1(t) + A_2 z_2(t) + B_1 u(t) \\ \dot{z}_2(t) = A_3 z_1(t) + A_4 z_2(t) + B_2 u(t) + F_2 f_a(z,t) \\ y(t) = Cz(t) \end{cases} \tag{14}$$

where, z_1 and z_2 are non-output and output states vectors in the new coordinate system respectively. $z_1 \in R^{(n-p)\times 1}$, $z_2 \in R^{p\times 1}$.

A.2: Observer Design

In this section, a TSMO is designed for the linearized system using [24]. The observer state equations are defined as follows:

$$\begin{cases} \dot{\hat{z}}_1(t) = A_1\hat{z}_1(t) + A_2\hat{z}_2(t) + B_1 u(t) + l_1 e_y(t) + l_2 \upsilon^{\frac{\alpha}{\beta}} \\ \dot{\hat{z}}_2(t) = A_3\hat{z}_1(t) + A_4\hat{z}_2(t) + B_2 u(t) + l_3 e_y(t) + l_4 \upsilon \\ \hat{y}(t) = C\hat{z}(t) \end{cases} \tag{15}$$

α and β are odd integers ($\alpha < \beta$). The observer's coefficients are obtained as follows:

$$l_1 = -A_2, l_2 = \begin{bmatrix} l_{21} & 0_{1\times 2} \end{bmatrix}, l_3 = -A_4 + A_{4s}, l_4 = -\phi \tag{16}$$

where $A_{4s} \in R^{3\times 3}$ is a desired stable matrix and $\phi = diag(\rho_1, \rho_2, \rho_3)$. ρ_1, ρ_2 and ρ_3 are positive scalars and

$$l_{21} = -\frac{p_1^{\frac{\alpha-\beta}{2\beta}}}{A_{31}} \tag{17}$$

Since A_1 is stable, two positive scalars p_1 and q_1 exist that satisfy the following condition:

$$p_1 A_1 + A_1^T p_1 = 2A_1 p_1 \le -q_1 \tag{18}$$

$A_{4s} \in R^{3\times 3}$ is a desired stable matrix. Moreover, A_3 is partitioned as $A_3 = \begin{bmatrix} A_{31} & A_{32} \end{bmatrix}^T$. The error vectors are defined as:

$$\begin{cases} e_1 = \hat{z}_1 - z_1 \\ e_2 = e_y = \hat{z}_2 - z_2 \end{cases} \tag{19}$$

e_1 and e_2 are non-output and output variables estimation errors. The convergence of e_1 and e_2 to zero in a finite time is proved using the Lyapunov functions $\bar{V}_1 = p_1\bar{e}_1^2$ and $V_2 = \frac{1}{2}e_2^T e_2$ [24]. $\bar{e}_1$ is defined as $\bar{e}_1 = A_{31}e_1$.

Using an inverse coordinate transformation, the observer's equations in the original coordinate system are as follows:

$$\begin{cases} \dot{\hat{x}}(t) = \bar{A}_L\hat{x}(t) + \bar{B}u(t) + R_1 e_y(t) + R_2\upsilon(t) + R_3\upsilon^{\frac{\alpha}{\beta}}(t) \\ y(t) = \bar{C}\hat{x}(t) \end{cases} \tag{20}$$

where:

$$\upsilon = \begin{bmatrix} sign(e_{21}) \\ sign(e_{22}) \\ sign(e_{23}) \end{bmatrix}, sign(e_i) = \frac{e_i}{|e_i| + \delta_i} \tag{21}$$

δ_i is a small positive constant, which is considered in order to prevent zero denominators. The observer's coefficients are:

$$R_1 = T_L^{-1}\begin{bmatrix} l_1 \\ l_3 \end{bmatrix}, R_2 = T_L^{-1}\begin{bmatrix} 0 \\ l_4 \end{bmatrix}, R_3 = T_L^{-1}\begin{bmatrix} l_2 \\ 0 \end{bmatrix} \tag{22}$$

Considering the Lyapunov function V_2, the following inequality holds [24]:

$$\dot{V}_2 < -\sigma_1\|e_2\| \tag{23}$$

σ_1 is a positive design scalar. V_2 can be written as $V_2 = \frac{1}{2}\|e_2\|^2$. Therefore, using (23):

$$\frac{dV_2}{2\sqrt{V_2}} < -\frac{\sigma_1}{\sqrt{2}}dt \tag{24}$$

Defining t_2 as the e_2 convergence time to zero and integrating (24), the convergence time of output states estimation errors to zero is calculated as the below equation:

$$t_2 < \frac{\sqrt{2V_2(0)}}{\sigma_1} \tag{25}$$

In time duration of t_2 seconds, V_2 will become zero and sliding motion will occur on $e_2 = 0$.

Using $\bar{V}_1$, the following equation is obtained [24]:

$$\dot{\bar{V}}_1 < -2\rho_1^{-\frac{\alpha}{\beta}}\left(p_1\bar{e}_1^2\right)^{\frac{\alpha+\beta}{2\beta}} \tag{26}$$

Integrating (26), the convergence time of non-output states estimation errors to zero is calculated as the below equation:

$$t_1 < \frac{\beta}{\beta-\alpha}\rho_1^{-\frac{\alpha}{\beta}}\bar{V}_1^{\frac{\beta-\alpha}{2\beta}}(0) \tag{27}$$

After convergence of e_2 to zero, in time duration of

t_1, $V_1(t_1)$ will become zero and sliding motion will occur on $e_1 = e_2 = 0$. Therefore, $V_1(0)$ is the initial value of V_1, after convergence of e_2 to zero.

A.3: Fault Estimation

The fault is estimated as follows:

$$\hat{f}_a = -F_2^+ \phi \upsilon_{eq} \quad (28)$$

υ_{eq} is equivalent injection switching term to establish sliding motion on $e = 0$, which is calculated using (21) and $F_2^+ = \left(F_2^T F_2\right)^{-1} F_2^T$.

Results and Discussion

In this section, wind turbine controllers and TSMO are implemented in order that the control objectives are achieved and also output estimation errors converge to zero in finite time.

A. Wind Turbine, Controllers, and TSMO Simulation

The $3kW$ PMSG wind turbine, which is introduced in section 2, the controllers, and the observer are simulated. The system's state-space equations, maximum power capture controller (2), pitch controller (3), and TSMO are simulated in Simulink. Then, the states, outputs, and fault are estimated. The optimum value of the power coefficient of the WT proportional to the optimum TSR $\lambda^* = 7.14$ is $C_{P_{\max}} = 0.439$ [26]. Karman spectrum model with a mean wind speed of 8 meters per second is considered as the wind model. Wind rated speed equals to $10.5 \, m/s$ and simulation is implemented in the low-speed region for 10 seconds. The parameters of the wind turbine are given in Table 1.

Table 1: 3kW PMSG wind turbine parameters [27]

PMSG	Drive train and rotor
$p = 3$, $R_s = 3.3\ \Omega$ $\Phi_m = 0.4382\ \text{Wb}$ $L_d = 41.56\ \text{mH}$ $L_q = 41.56\ \text{mH}$ $R_{\text{ln}} = 80\ \Omega$, $V_s = 380\,\text{V}$ $\rho = 1.25\ \text{kg/m}^3$	Gear ratio: $N_g = 7$ Moment of inertia: $J_h = 0.5042\ \text{kg.m}^2$ Efficiency: $\eta = 1$ Blade length: $R = 2.5\ \text{m}$

The inductance of the equivalent load equals to $L_L = 0.08\ \text{H}$ [28]. The control accuracy of pitch angle equals to 0.3 degrees [29]. Pitch rate is between ± 2 and ± 18 degrees per second practically [30]. In this research, the maximum value of the pitch rate is considered as ± 15 degrees per second. Using (1), the pitch actuator's time constant equals to $\tau_\beta = 0.3/15 = 0.02$.

B. Linearized Systems, Controllers, and Observer Simulation

Using the system of equations of (5) the equilibrium point is:

$$x_0 = \begin{bmatrix} -1.38 & 4.66 & 0 & 8.46 \end{bmatrix}^T \quad (29)$$

The stability of this equilibrium point is investigated using the matrix $\bar{A}_L$. Since all eigenvalues of the matrix $\bar{A}_L$ lie in the left half plane, this equilibrium point is stable. According to the condition A_2 in (10), it is necessary to increase the number of sensors in order that the observer can estimate the states and the fault. Hence, the number of measurable outputs are increased to three. Therefore, two sensors must be added to the wind turbine system in order to measure the first and second outputs. It is not required to add an additional sensor to measure the generator speed, which is the third output, because it is already measured in the wind turbine systems.

$$A_2 : 2p \ge n + q \quad \rightarrow \quad A_2 : 2 \times 3 \ge 4 + 1$$

Hence, $\bar{C}$ matrix changes as below:

$$\bar{C} = \begin{bmatrix} 0 & 1 & 0 & 0 \\ 0 & 0 & 1 & 0 \\ 0 & 0 & 0 & 1 \end{bmatrix} \quad (30)$$

The following maximum power controller is used in the simulations:

$$G_{CMP}(s) = 2.542 + 2.319\frac{1}{s} + 0.178\frac{130.843}{1 + 130.843\frac{1}{s}} \quad (31)$$

The pitch angle controller (3) is designed as follows:

$$G_{CP}(s) = 2 + \frac{0.05}{s} \quad (32)$$

According to (11) the coordinate transformation matrix T_L is:

$$T_L = \begin{bmatrix} -10 & 1 & 0 & 0 \\ 0 & 1 & 0 & 0 \\ 0 & 0 & 1 & 0 \\ 0 & 0 & 0 & 1 \end{bmatrix} \quad (33)$$

The value of other parameters of the observer are chosen as below:

$$\begin{aligned} &\rho_1 = \rho_2 = \rho_3 = 1000 \\ &\alpha = 3, \beta = 5 \\ &p_1 = 1, q_1 = 1 \\ &A_{4s} = diag\{-1, -2, -3\} \\ &\delta_i = 0.01 \end{aligned} \quad (34)$$

The convergence time of output and non-output states equals to:

$$t_2 < \frac{\sqrt{0.076}}{50} = 5.51\times10^{-3}\,\mathrm{s} \tag{35}$$

$$t_1 < \frac{5}{2}1000^{-\frac{3}{5}}(2.538\times0.15)^{\frac{4}{10}} = 0.027\,\mathrm{s} \tag{36}$$

The simulation results are presented in Figs. 2 to 8:

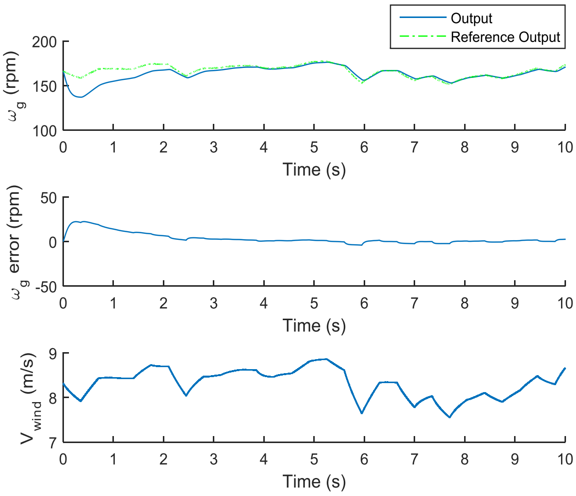

Fig. 2: Generator's reference speed, generator's speed, generator's speed tracking error, and wind speed.

According to Fig. 2, the generator speed converges to the desired output after 3 seconds using a PID controller. Using TSMO, state estimation errors converge to zero in finite time as represented in Figs 3 and 4.

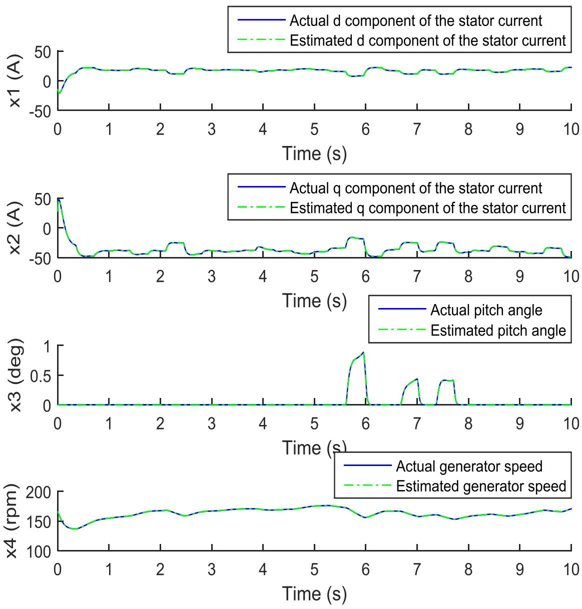

Fig. 3: Actual and estimated states.

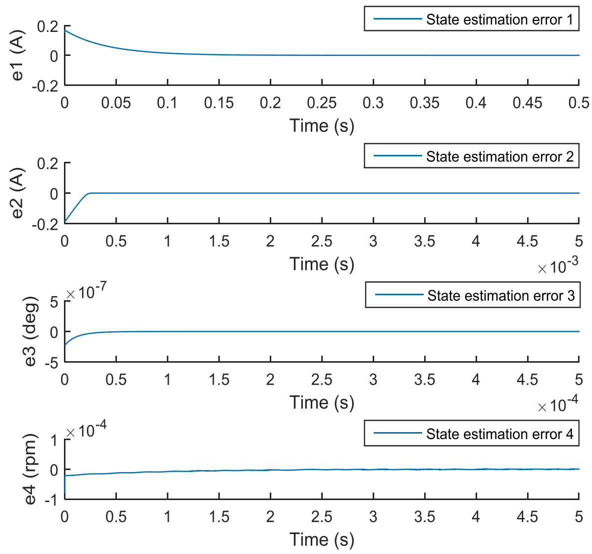

Fig. 4: State estimation errors (zoomed).

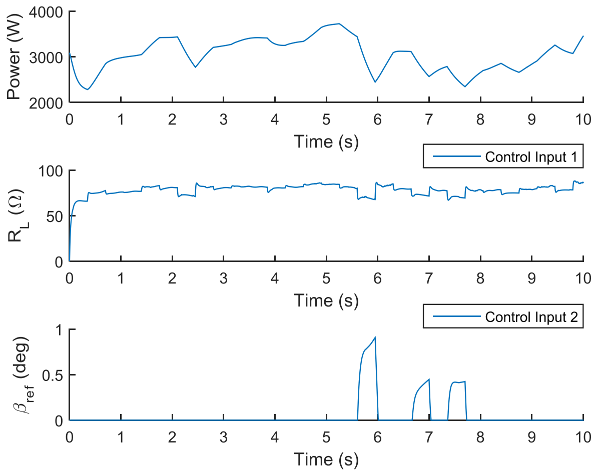

Fig. 5: Power and control inputs.

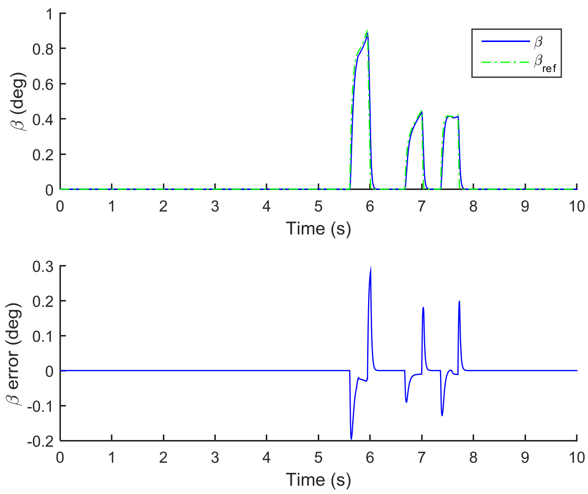

Fig. 6: Pitch angle, reference pitch angle, and pitch angle error with respect to reference pitch angle.

According to Figs. 5 and 6, the wind turbine's power is variable between 2 and 4 kW. In addition, in order for the desired control objective, which is maximum power capturing, to be achieved, R_L should variate between 65 Ω and 90 Ω and β_{ref} should be between 0 and 1 deg.

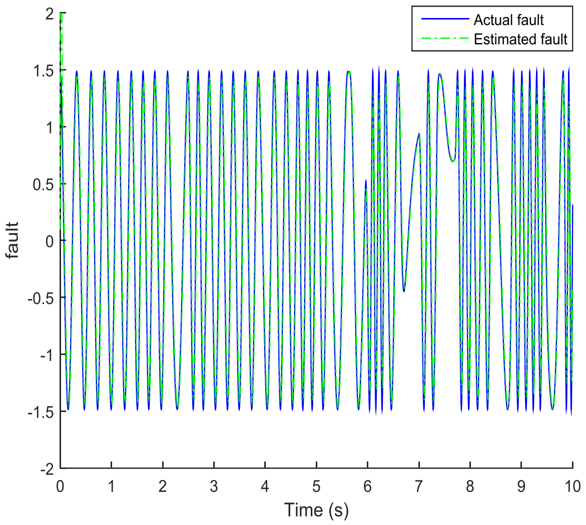

Fig. 7: Actual and estimated fault.

As it is presented in Fig. 7, the WT fault is detected and the actual fault and estimated fault diagrams approximately coincide.

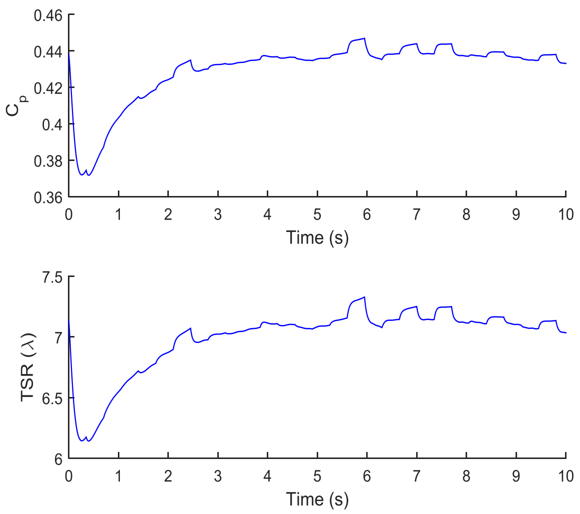

Fig. 8: Power coefficient and TSR.

According to Fig. 8, after a time duration of 3 seconds, in which the system's output traces the desired output, the power coefficient and TSR have variations in the ranges close to their optimum values, which are 0.439 and 7.14, respectively. Therefore, the maximum power is captured.

Furthermore, both measured and unmeasured states and BIF are estimated in a finite time.

Conclusion

According to simulation results, which are presented in the previous section, using TSMO, BIF is detected and the states are estimated. BIF is modeled as a sinusoidal function with a frequency equal to the rotating frequency of the wind turbine shaft. The frequency of BIF is time-varying because of the time-varying nature of wind speed.

Using the designed observer, the sinusoidal function of BIF with variable frequency is estimated as well. TSMO's advantage in comparison to sliding mode observer (SMO) is that using TSMO not only output estimation errors, but also non-output estimation errors converge to zero in finite time.

In future research works, a TSMO could be designed in order to estimate the states and detect the fault considering nonlinear state-space equations of the PMSG wind turbine.

Author Contributions

S. Khodakaramzadeh, worked on conceptualization, developed the methodology and simulations, and edited/reviewed the paper. M. Ayati is the supervisor, worked on conceptualization, developed the methodology and he edited/reviewed the paper. M. R. Ha'iri-Yazdi is the supervisor and he edited the paper.

Acknowledgment

The author gratefully acknowledges the (American Control Conference, P. F. Odgaard and K. E. Johnson, for their work on WT modeling), (Automatica, C.P. Tan, X. Yu, Z. Man, for their work on terminal sliding mode observers), and (Renewable Energy, M. Rahnavard, M. Ayati, M. R. Hairi-Yazdi, and M. Mousavi, for their work on the finite-time fault estimation of WT).

Conflict of Interest

The authors declare no potential conflict of interest regarding the publication of this work. In addition, the ethical issues including plagiarism, informed consent, misconduct, data fabrication and, or falsification, double publication and, or submission, and redundancy have been completely witnessed by the authors.

Abbreviations

BIF	Blade Imbalance Fault
DFIG	Doubly Fed Induction Generator
EMD	Empirical Mode Decomposition
FDS	Fault Detection System
FQL	Fuzzy Q-Learning
GEP	Gene Expression Programming
OM	Operation and Maintenance

PMSG	Permanent Magnet Synchronous Generator
SMO	Sliding Mode Observer
TSMO	Terminal Sliding Mode Observer
TSR	Tip Speed Ratio
WECS	Wind Energy Conversion System
WT	Wind Turbine

References

[1] M. Rahnavard, M. Ayati, M.R. Hairi Yazdi, “Robust actuator and sensor fault reconstruction of wind turbine using modified sliding mode observer,” Trans. Inst. Meas. Control, 41(6): 1504–1518, 2018.

[2] M. HojatyDana, M. AlizadehPahlavani, “Control strategies for performance assessment of an autonomous wind energy conversion system,” J. Electr. Comput. Eng. Innov., 2(1): 15–20, 2014.

[3] H. Malik, S. Mishra, “Application of LVQ network in fault diagnosis of wind turbine using turbsim , FAST and simulink,” in Proc. Michael Faraday IET Int. Summit: 474–480, 2015.

[4] M.L. Corradini, A. Cristofaro, S. Pettinari, “Diagnosis and accommodation of faults affecting the PMSG in variable-speed sensorless wind turbines - A deterministic approach,” 2014 Eur. Control Conf. (ECC): 1957–1962, 2014.

[5] C.C. Ciang, J. Lee, H. Bang, “Structural health monitoring for a wind turbine system : a review of damage detection methods,” Meas. Sci. Technol., 19(12), 2008.

[6] S.M. Miryousefi Aval, A. Ahadi, “Wind turbine fault diagnosis techniques and related algorithms,” Int. J. Renew. Energy Res., 6(1): 80–89, 2016.

[7] B. Lu, Y. Li, X. Wu, Z. Yang, “A review of recent advances in wind turbine condition monitoring and fault diagnosis,” presented at the 2009 IEEE Power Electron. Mach. Wind Appl., Lincoln, NE, USA, 2009.

[8] D. Lu, W. Qiao, “Frequency Demodulation-Aided Condition Monitoring for Drivetrain Gearboxes,” presented at the 2013 IEEE Transp. Electrif. Conf. Expo, Detroit, MI, USA, 2013.

[9] N.M. A. Freire, J.O. Estima, A.J. M. Cardoso, “A new approach for current sensor fault diagnosis in pmsg drives for wind energy conversion systems,” in Proc. 2012 IEEE Energy Convers. Congr. Expo.:2083–2090, 2012.

[10] M. Rahnavard, M.R. Hairi Yazdi, M. Ayati, “On the development of a sliding mode observer- based fault diagnosis scheme for a wind turbine benchmark model,” J. Energy Equipments Syst., 5(1): 13–26, 2017.

[11] J. Guo, S. Lu, C. Zhai, Q. He, “Automatic bearing fault diagnosis of permanent magnet synchronous generator in wind turbine subjected to noise interference,” Meas. Sci. Technol., 29(2), 2017.

[12] R.K. Ibrahim, S. Watson, “Condition Monitoring of Permanent Magnet Synchronous Generator for wind turbine applications,” in Proc. 2016 3rd Conf. Control Fault-Tolerant Syst.: 648–653, 2016.

[13] M.L. Corradini, G. Ippoliti, G. Orlando, “Sensorless fault-tolerant control of VS Wind Turbines maximizing efficiency in the presence of electrical faults,” in Proc. 2015 IEEE 54th Annu. Conf. Decis. Control: 682–687, 2015.

[14] P.F. Odgaard, K.E. Johnson, “Wind turbine fault detection and fault tolerant control - an enhanced benchmark challenge,” 2013 Am. Control Conf.: 4447–4452, 2013.

[15] E. Sales-Setien, I. Penarrocha, D. Dolz, R. Sanchis, “Fault detection in the blade and pitch system of a wind turbine with H2 PI observers,” J. Phys. Conf. Ser., 659: 1-10, 2015.

[16] X. Gong, W. Qiao, “Imbalance fault detection of direct-drive wind turbines using generator current signals,” IEEE Trans. Energy Convers., 27(2): 468–476, 2012.

[17] H. Malik, S. Mishra, “Proximal support vector machine (PSVM) based imbalance fault diagnosis of wind turbine using generator current signals,” J. Energy Procedia, 90: 593–603, 2016.

[18] H. Malik, S. Mishra, “Application of Fuzzy Q Learning (FQL) technique to wind turbine imbalance fault identification using generator current signals,” presented at the 2016 IEEE 7th Power India Int. Conf., Bikaner, India, 2016.

[19] H. Malik, S. Mishra, “Application of Gene Expression Programming (GEP) to investigate the health condition of direct-drive wind turbine,” presented at the 2016 7th India Int. Conf. Power Electron., Patiala, India, 2016.

[20] S. Boulouma, H. Belmili, S. Labiod, “Robust adaptive maximum power capture control scheme for a PMSG based WECS,” presented at the 2015 4th Int. Conf. Electr. Eng. ICEE 2015, Boumerdes, Algeria, 2015.

[21] X. Tong, X. Zhao, “Power generation control of a monopile hydrostatic wind turbine using an H∞ loop-shaping torque controller and an LPV pitch controller,” IEEE Trans. Control Syst. Technol., 26(6): 2165–2172, 2017.

[22] N.A. Orlando, M. Liserre, R.A. Mastromauro, A.D. Aquila, “A survey of control issues in PMSG-based small wind-turbine systems,” IEEE Trans. Ind. informatics, 9(3): 1211–1221, 2013.

[23] J. Hang, J. Zhang, M. Cheng, “Fault diagnosis of wind turbine using control loop current signals,” in Proc. 2014 IEEE Energy Convers. Congr. Expo.: 3119–3124, 2014.

[24] M. Rahnavard, M. Ayati, M.R. Hairi Yazdi, M. Mousavi, “Finite time estimation of actuator faults, states, and aerodynamic load of a realistic wind turbine,” Renew. Energy, 130: 256–267, 2019.

[25] M. Mousavi, M. Rahnavard, S. Haddad, “Observer based fault reconstruction schemes using terminal sliding modes,” Int. J. Control, 93(4): 881–888, 2018.

[26] S. M. Muyeen, J. Tamura, T. Murata, Stability Augmentation of a Grid-connected Wind Farm. Springer, 2009.

[27] I. Munteanu, A. Bratcu, N. Cutululis, E. Ceanga, Optimal Control of Wind Energy Systems: Toward a Globlal Approach. Springer, 2008.

[28] H.M. Nguyen and D. S. Naidu, “Direct fuzzy adaptive control for standalone wind energy conversion systems,” presented at the World Congr. Eng. Comput. Sci., San Francisco, USA, 2012.

[29] S. Baburajan, “Improving the efficiency of a wind turbine system using a fuzzy-pid controller,” presented at the 2018 Adv. Sci. Eng. Technol. Int. Conf., Dubai, United Arab Emirates, 2018.

[30] M.A. Mosa, A.A. Elsyed, A.M.A. Amin, A.M.A. Ghany, “Variable speed wind turbine pitch angle controller with rate limiter anti-windup,” presented at the 2016 Eighteenth Int. Middle East Power Syst. Conf., Cairo, Egypt, 2016.

Biographies

Shabnam Khodakaramzadeh was born in Tehran, Iran, in 1993. She received her B.Sc. from Sharif University of Technology in 2016 and M.Sc. from University of Tehran in 2018, both in mechanical engineering. Her research interests include control, automation, and fault diagnosis.

Moosa Ayati received his B.Sc. degree from Isfahan University of Technology, Isfahan, Iran, in 2004, and his M.Sc. and Ph.D. degrees in 2006 and 2011 from K. N. Toosi University of Technology, Tehran, Iran, all in Electrical Engineering with the first rank honors. He spent two years as a Post-Doctoral Fellow at the University of Tehran School of Electrical Engineering, College of Engineering, Tehran, Iran, working on fault detection systems. He is currently head of the Advanced Instrumentation Laboratory (AIL) and an Associate Professor with the control division, School of Mechanical Engineering, College of Engineering, at University of Tehran, Tehran, Iran. His area of interest includes adaptive control and system identification, fault detection systems, instrumentation and industrial automation, Mechatronics, and hybrid systems. Professor Ayati is a member of Iranian Society of Instrumentation and Control, Iranian Society of Mechanical Engineers, and National Society of Mechatronics.

Mohammad Reza Hairi Yazdi received his B.Sc. and M.Sc. degrees in Mechanical Engineering from Amir Kabir University of Technology, Tehran, Iran in 1985 and 1987 respectively. He received his Ph.D. degree from Imperial College London in 1992 and since then he has been at the University of Tehran, Tehran, Iran where he is now a Professor at the School of Mechanical Engineering. His main research interests include design, simulation, manufacturing and control of dynamic systems.

How to cite this paper:

S. Khodakaramzadeh, M. Ayati, M.R. Ha'iri-Yazdi, "Fault diagnosis of a permanent magnet synchronous generator wind turbine," J. Electr. Comput. Eng. Innovations, 9(2): 143-152, 2021.

DOI: 10.22061/JECEI.2020.7424.408

URL: http://jecei.sru.ac.ir/article_1512.html